Journal of Materials Chemistry B

Molecular Simulations and Understanding of Antifouling Zwitterionic Polymer Brushes

Journal:	*Journal of Materials Chemistry B*
Manuscript ID	TB-ART-02-2020-000520.R1
Article Type:	Paper
Date Submitted by the Author:	11-Mar-2020
Complete List of Authors:	Liu, Yonglan; University of Akron, Chemical, Biomolecular, and Corrosion Engineering Zhang, Dong; University of Akron, Chemical, Biomolecular, and Corrosion Engineering Ren, Baiping; University of Akron, Chemical, Biomolecular, and Corrosion Engineering Gong, Xiong; University of Akron, Polymer Eng Xu, Lijian; Henan University of Technology Feng, Zhangqi; Nanjing University of Science and Technology, Chemicobiology and Functional Materials Institute Chang, Yung; Chung Yuan Christian University, Chemical Engineering He, Yi; Zhejiang University, College of Chemical and Biological Engineering Zheng, Jie; University of Akron, Chemical, Biomolecular, and Corrosion Engineering

Molecular Simulations and Understanding of Antifouling Zwitterionic Polymer Brushes

Yonglan Liu[1¶], Dong Zhang[1¶], Baiping Ren[1], Xiong Gong[2], Lijian Xu[3], Zhang-Qi Feng[4], Yung Chang[5], Yi He[6], and Jie Zheng[1,2*]

[1]Department of Chemical, Biomolecular, and Corrosion Engineering
The University of Akron, Ohio 44325, USA

[2]Department of Polymer Engineering
The University of Akron, Ohio 44325, USA

[3]Hunan Key Laboratory of Biomedical Nanomaterials and Devices
College of Life Science and Chemistry
Hunan University of Technology, Zhuzhou 412007, P. R. China

[4]School of Chemical Engineering
Nanjing University of Science and Technology, Nanjing, China, 210094

[5]Department of Chemical Engineering and R&D Center for Membrane Technology
Chung Yuan Christian University, Taoyuan 320, Taiwan

[6]College of Chemical and Biological Engineering
Zhejiang University, Hangzhou, Zhejiang 310027, China

¶ The authors contribute equally to this work.
*Corresponding Author: zhengj@uakron.edu

Abstract

Zwitterionic materials are an important class of antifouling biomaterials for various applications. Despite such desirable antifouling properties, molecular-level understanding of the structure-property relationship associated with surface chemistry/topology/hydration and antifouling performance still remains to be elucidated. In this work, we computationally studied the packing structure, surface hydration, and antifouling property of three zwitterionic polymer brushes of poly(carboxybetaine methacrylate) (pCBMA), poly(sulfobetaine methacrylate) (pSBMA), and poly((2-(methacryloyloxy)ethyl) phosporylcoline) (pMPC)) brushes and a hydrophilic PEG brush using a combination of molecular mechanics (MM), Monte Carlo (MC), molecular dynamics (MD), and steered MD (SMD) simulations. We for the first time determined the optimal packing structures of all polymer brushes from a wide variety of unit cells and chain orientations in a complex energy landscape. Under optimal packing structures, MD simulations were further conducted to study the structure, dynamics, and orientation of water molecules and protein adsorption on four polymer brushes, while SMD simulations to study the surface resistance of polymer brushes to a protein. Collective results consistently revealed that three zwitterionic brushes exhibited the stronger interactions with water molecules and the higher surface resistance to a protein than PEG brush. It was concluded that both carbon space length between zwitterionic groups and the nature of the anionic groups have a distinct effect on the antifouling performance, leading to a following antifouling ranking of pCBMA > pMPC > pSBMA. This work hopefully provides some structural insights into the design of new antifouling materials beyond traditional PEG-based antifouling materials.

Keywords: Zwitterionic materials, Polymer brushes, Molecular simulation, Surface hydration, Antifouling property

1. Introduction

Zwitterionic polymers possess a unique structural feature, i.e., a combination of the equal number of cationic groups (e.g. phosphonium, pyridinium, imidazolium and quaternary/tertiary/secondary/primary ammonium groups) and anionic groups (e.g. carboxylate, sulfonate, phosphate groups) in the same pendant motif[1-2]. Such unique structural feature also empowers zwitterionic polymers with different functional properties, including overall charge neutrality, high hydrophilicity, strong dipole pairs, and anti-polyelectrolyte effect[3]. Zwitterionic polymers can be fabricated into different structural forms of brushes[4-5], hydrogels[6-8], membranes[9], films[10], particles[11], and coatings[12], with different functions of antifouling[7-8, 12], stimuli-responsive[13-16], antibacterial[8], self-healing[17], lubrication[18-19] properties for different applications of marine coatings[12], wound dressings[20], drug/gene delivery carriers[21-22], biosensors[23-24], and implants[7]. Among these diverse structures, functions, and applications, zwitterionic polymers are still well recognized by their excellent antifouling property and used as antifouling coatings, comparable or even superior to poly(ethylene glycol) (PEG)-based coatings[25-27]. The most common zwitterionic moieties include carboxybetaine (CB), sulfobetaine (SB), and phosphatidylcholine (PC), which are often used to be polymerized into polymer brushes via the grafting-to or grafting-from methods. The antifouling property of zwitterionic polymers is generally accepted by the water barrier principle, where zwitterionic ion pairs strongly attract neighboring waters via electrostatically induced interactions to form a tightly and stably bounded water layer on polymer brushes[28], which would induce to form a physical and energy barrier to prevent the adsorption of proteins, cells, and bacteria, in assistance with steric repulsion of polymer chains[5, 8, 29-32].

While experimental studies on zwitterionic brushes have been intensively conducted to demonstrate their surface resistance to proteins, cells, bacteria, and other micro/macroorganisms[5, 33-36], it remains a great challenge to real-time quantify the changes in dynamic and interactive behavior of polymer brush, interfacial water, protein conformation/orientation at polymer/water/protein interface. Computer simulations can provide further insights into the structural, dynamical, and interaction properties at polymer-water and polymer-protein interfaces with an atomic resolution that is difficult to achieve experimentally. While there are some computational studies of zwitterionic polymer systems with main focus on surface hydration and protein interaction of zwitterionic monomers[37-38] and zwitterionic-terminated self-assembled monolayers[4], antifouling mechanism of zwitterionic monomer-grafted membranes[39-40], and antifouling and mechanical properties of zwitterionic hydrogels[41] using molecular dynamics (MD) simulations, very few studies have been conducted to simulate the protein adsorption/desorption on zwitterionic brushes in the presence of explicit water. Early molecular simulations of zwitterionic materials mainly focused on the interfacial water behaviors on PC-terminated self-assembled monolayers (PC-SAMs), as in comparison with EG-, OH-, and CH_3-terminated SAMs[42-44]. It was found that hydrophilic or zwitterionic-terminated SAMs including EG-, OH-, and PC-SAMs induced a stronger interaction with interfacial water molecules than hydrophobic CH_3-SAM[25, 43, 45-47], indicating that surface hydration is considered as a crucial factor for antifouling performance because the strongly hydration layer near the surface prevents the adhesion of foreign substances. Later, with significant increase in computer power, MD simulations

allow to model and simulate more complex and larger polymer-grafted surfaces in the absence and presence of foulants. Cheung et al.[48] applied MD simulations to examine the effect of grafting density on the conformation and hydration properties of a series of zwitterionic "peptoids" brushes. They found that chain flexibility and water density around peptoid brush chains were promoted by charged monomers/residues at "low" and "intermediate" grafting densities, but were suppressed at high grafting densities due to free volume effects. Liu et al.[39] modelled a zwitterionic DMAPs-grafted PVDF membrane (e.g. PVDF-g-DMAPS membrane) and used this zwitterionic-coating membrane to study the fouling process of a sodium alginate in water molecules and $CaCl_2$ ions. Hydrophilic property and electrostatic repulsion of PVDF-g-DMAPS membrane are the two dominate but competing factors to control antifouling capability at different zwitterionic DMAPS grafting ratios. Xiang et. al[49] computationally studied the surface hydration and antifouling behavior of poly(sulfobetaine)-grafted (pSB) brushes using steered MD simulations. They observed the grafting-density-dependent antifouling behavior, i.e., surface resistance to protein is attributed to the surface hydration layer at highly grafted pSB brushes, but steric repulsion as induced by protein compression on intermediate- and low-grafted pSB brushes.

While the above-mentioned simulations and experiments have examined the structural dependent of grafting density on a surface hydration, polymer dynamics, and their correlation with antifouling performance, they all did not address the packing structure of zwitterionic polymer brushes. Since most of polymer brushes are prepared via the two-step surface-initiated atom transfer radical polymerization (SI-ATRP) by first coating an initiator-SAM on the gold substrate, followed by ATRP to gradually grow polymer chains to form polymer brushes with well-controlled thickness and roughness. Thus, the packing structure of these polymer brushes is solely determined by the packing structure of underlying initiator-SAM on the gold substrate, in which polymer chains have been often assumed to adopt the conventional $\sqrt{3}\times\sqrt{3}R30^o$ lattice structure with a chain-chain separation distance of 4.95 Å via typical sulfur-gold (S-Au) bonds. Such conventional $\sqrt{3}\times\sqrt{3}R30^o$ lattice structure can well describe the packing structure of polymer brushes with small terminal or pendant groups (e.g., $-CH_3$, -EG, -OH, and COOH). However, it still remains unknown whether this small lattice structure can be also applied to other polymer brushes with much larger pendant groups. Our previous work has found that even for rigid and short SAMs, PC-SAMs prefer to adopt a larger $\sqrt{7}\times\sqrt{7}R19^o$ lattice structure, instead of $\sqrt{3}\times\sqrt{3}R30^o$ lattice structure, due to the larger size and stronger polarity of zwitterionic PC groups[44].

Currently, there is little information on the packing structure of zwitterion polymer brushes, which prevents a better understanding of the structural-dependence relationship between surface hydration and protein resistance on a molecular scale. To bridge this gap, herein we performed different molecular dynamics simulations to computationally study the packing structure, surface hydration, and surface resistance to protein of the three zwitterionic polymer brushes of poly(carboxybetaine methacrylate) (pCBMA), poly(sulfobetaine methacrylate) (pSBMA), and poly((2-(methacryloyloxy)ethyl) phosporylcoline) (pMPC)) brushes, as well as hydrophilic poly(ethylene glycol) (PEG) brush for comparison. Firstly, we studied and determined optimal lattice structures of four polymer brushes on Au substrate at their lowest energy states from a large energy landscape

using molecular mechanics (MM) simulations. Different from PEG brush, three zwitterionic polymer brushes are more likely to undergo large conformational changes and involve more complex inter- and intra-interactions (e.g. charge-charge, charge-dipole, and dipole-dipole interactions due to their long side chains and the larger zwitterionic groups, both of which would require the larger lattice structures to accommodate the packing structure and interactions between polymer chains. Then, upon obtaining optimal lattice structures, surface hydration and surface resistance to protein of the four polymer brushes were examined and compared using both conventional molecular dynamics (MD) and steered MD (SMD) simulations. Collective MD data from RDFs, coordination number, self-diffusion, and mean residence time of interfacial water molecules revealed that pCBMA, pSBMA, and pMPC brushes had the stronger and more stable interactions with interfacial water molecules than PEG brush. SMD further demonstrated the existence of repulsive force derived from three zwitterionic brushes to resist protein adsorption. Among four polymer brushes, the strength of surface hydration and protein resistance decreased in the order of pCBMA > pMPC > pSBMA > PEG. Our simulation works for the first time determined the optimal packing structure of zwitterionic brushes and provided a more accurate description of packing structural dependent relationship between surface hydration and antifouling property of zwitterionic polymer brushes at atomic level, which helps to design more effective antifouling materials and coating surfaces.

2. Materials and Methods

2.1. Force Field Parameters

We developed the CHARMM-format force field parameters of CBMA and SBMA monomers using the ParaChem tool (https://cgenff.paramchem.org/)[50] and obtained the force field parameters of MPC and EG monomers from both CHARMM36 lipid paramters[51] and CHARMM35 ether parameters[52], respectively. The molecular structure of CBMA, SBMA, and MPC monomers are showed in **Figure 1** and their force field parameters in the CHARMM format were provided in **Table S1**. Lysozyme (LYZ, PDB ID: **7LYZ**)[53] was selected as a model protein to study of four different brushes due to extensive studies on its adsorption behavior on different surfaces. CHARMM27 parameter set with CMAP correction[54] was used to model the lysozyme, water (TIP3P model), and counter ions.

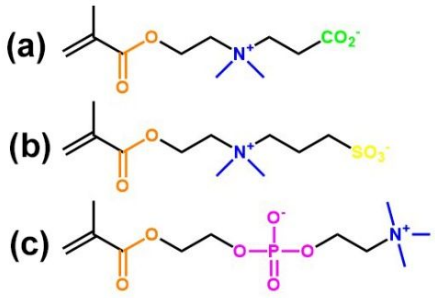

Figure 1. Molecular structures of (a) carboxybetaine methacrylate (CBMA), (b) sulfobetaine methacrylate (SBMA), and (c) (2-(methacryloyloxy)ethyl) phosporylcoline (MPC).

2.2. Model construction of polymer brushes

To study surface hydration of different polymer brushes, we constructed polymer brush models in the presence of the explicit TIP3P water model, including three zwitterionic polymer brush models (pCBMA, pSBMA, and pMPC) and a PEG model. For any given polymer brush model, single chain was firstly constructed by connecting 5 repeated carboxybetaine methacrylate (CBMA), sulfobetaine methacrylate (SBMA), (2-(methacryloyloxy)ethyl) phosporylcoline (MPC), or ethylene glycol (EG) monomers to an initiator on Au and then energy minimized in vacuum. Then, we applied molecular mechanics (MM) simulations to determine the optimal packing structure of different brushes. The optimal packing structure of these brushes primarily depends on the packing density and the orientation of brush chains. For any given minimized single chain of zwitterionic polymer or PEG brush, we created a 6×6 array of brush chains to model the packing structure of various polymer brushes by using 29 unit cells as a basic building block to describe their different packing densities and by rotating polymer chains from 0 to 360° by every 30° to describe different chain orientations. **Table 1** summarizes 29 unit cells and the corresponding geometric parameters (*a*, *b*, γ, and unit area), where *a* and *b* are the two vector lengths of different lattice structures and γ is the angle between *a* and *b*. The optimal packing structure of the four polymer brushes were determined at the lowest-energy state by comparing all possible packing structures from a combination of 29 unit cells and 12 chain rotations. Based on the optimal packing structure obtained above, we further created the much larger-size polymer brushes using a 15×9 array for zwitterionic polymer brush (135 zwitterionic polymer brush chains) and a 15×15 array for PEG (225 PEG chains) in the presence of the explicit TIP3P water molecules to study their surface hydration properties.

Table 1. Geometric parameters of 29 unit cells for a single brush chain

Lattice Name	*a* (Å)	*b* (Å)	γ (°)	Area (Å²)	Lattice Name	*a* (Å)	*b* (Å)	γ (°)	Area (Å²)
3	4.995	4.995	60	21.6	9b	8.652	7.630	79.1	64.8
4a	5.768	4.995	90	28.8	10a	9.990	10.398	43.9	72.0
4b	5.768	5.768	60	28.8	10b	10.398	7.630	65.2	72.0
5	7.630	4.995	70.9	36.0	10c	7.630	9.990	70.9	72.0
6a	8.652	4.995	90	43.2	10d	14.420	4.995	90	72.0
6b	9.990	4.995	60	43.2	10e	14.420	5.768	60	72.0
6c	8.652	5.768	60	43.2	10f	15.260	4.995	70.9	72.0
6d	5.768	7.630	79.1	43.2	11a	12.570	7.630	55.8	79.3
7	7.630	7.630	60	50.4	11b	7.630	10.398	90	79.3
8a	11.536	4.995	90	57.6	12a	11.360	8.652	61.6	86.4
8b	11.536	5.768	60	57.6	12b	8.652	10.398	73.9	86.4
8c	10.398	5.768	73.9	57.6	12c	14.980	7.630	48.2	86.4
8d	9.990	7.630	49.1	57.6	12d	11.360	7.630	85.6	86.4
8e	9.990	5.768	90	57.6	12e	8.652	9.990	90	86.4
9a	8.652	8.652	60	64.8					

2.3. Model construction of polymer brushes in the presence of a protein

Based on the optimal packing structures of the four polymer brushes, we will further examine the surface resistance ability to protein of the four polymer brushes by constructing the four polymer-protein models of polymer brushes with a lysozyme (pCBMA-LYZ, pSBMA-LYZ, pMPC-LYZ, and PEG-LYZ) in the presence of the explicit TIP3P water molecules and counter ions of NaCl. The calculated ionic strength was 1.85, 1.54, and 1.54 mol/L for pCBMA, pSBMA, and pMPC systems, respectively, which appears to be much higher than ionic strength of 0.295 mol/L in PBS solution. First, Monte Carlo (MC) simulations were performed to determine the optimal orientations of a lysozyme on different zwitterionic and PEG brushes. All polymer brushes were firstly energy minimized in the implicit solvent model while fixing sulfur atoms of initiators by using the conjugate gradient method for 1000 steps. Then, a lysozyme was placed at various separation distances of 3 to 10 Å above the minimized brushes with a random, initial orientation. During MC simulations, at a given separation distance between the lysozyme and polymer brushes, lysozyme was allowed to rotate freely around its center of mass for 5000 steps to find its optimal orientation on different polymer brushes, where brush surfaces were constrained in the x-y plane. The optimal orientation of lysozyme on distinct polymer brush was determined at the lowest interaction energy state between the brush and lysozyme. Upon determining the optimal orientation of a lysozyme on each polymer brush, these lysozyme-brushes configurations will be used as a starting pose to further study the adsorption process of a lysozyme on different brushes using molecular dynamics (MD) simulations and the surface resistance ability (i.e. repulsive force) of different brushes to a lysozyme using steered molecular dynamics (SMD) simulations. The details of MD and SMD simulations of a lysozyme on polymer brushes were described below.

From a modeling viewpoint, our and other brush models were constructed in a perfect flatness to eliminate any surface roughness effect on surface hydration and protein resistance. As shown in Figure below, the averaged brush heights for three zwitterionic brushes were well retained at a constant value, with almost undetectable fluctuation. Without surface roughness, molecular simulations can truly reflect the intrinsic antifouling property of polymer brush itself. From an experimental viewpoint, surface roughness is always a factor to influence surface hydration and protein interactions. We and other researchers have reported that either the flat surface or nanopatterned surfaces have the much better antifouling performance than randomized surface roughness[55-61].

2.4. MD Simulation Details

Prior to equilibrium and production MD simulations, multiple energy minimizations were performed to remove bad contacts and relax systems for each polymer brush model with or without a lysozyme: (i) conjugate gradient minimization was performed by constraining brush chains and a lysozyme to relax water molecules for 5000 steps; (ii) additional 5000-step minimization was carried out to relax all atoms with fixing only sulfur atoms; (iii) a short 0.5-ns MD simulations with time step of 1 fs was conducted to relax water molecules and ions with atoms of brush chains and lysozyme being fixed; (iv) another 0.5-ns MD simulations with fixing sulfur atoms at time step of 1 fs.

For conventional MD simulations, they were performed using all-atom NAMD 2.12 package[54] with CHARMM force field under a NVT (constant number of atoms, constant volume, and constant temperature) ensemble and 3D periodic boundary condition. The temperature was maintained at 298 K using Langevin thermostat method with a damping coefficient of 1 ps^{-1}. All covalent bonds including hydrogen bonds were constrained by RATTLE method, so that velocity Velert method was performed to integrate Newton motion equation with a larger timestep of 2-fs. For SMD simulations, lysozyme was firstly placed above the brushes with a separation distance of 14 Å. Then, a harmonic force with a force constant of 15 kcal/(mol*A^2) was applied to the center of mass of lysozyme by pulling the lysozyme towards the brushes at a constant velocity of 0.05 m/s using the NAMD 2.12 package[54]. During this puling process, a total of force acting on the lysozyme was real-time recorded. For both MD and SMD simulations, long-range electrostatic potentials were calculated by Particle Mesh Ewald (PME) with the grad space of 0.5 Å, while short-range van der Waals (VDW) potentials were estimated by the switching function with a twin-range cutoff at 12 Å and 14 Å. All MD trajectories were saved every 2 ps for further analysis.

3. Result and Discussion

3.1. Optimal packing structures of zwitterionic polymer and PEG Brushes

The packing structure of a polymer brush is generally described by packing density and chain orientation, both of which are critical for the physicochemical properties of the polymer brush[62]. Briefly, regarding packing density, we first used a total of twenty-nine unit cells with different sizes and shapes to separately construct twenty-nine 6×6 assays (containing 36 polymer chains) to model different packing densities of the four polymer brushes. **Figure 2** shows the twenty-nine unit cells and **Table 1** summarizes their geometric parameters (*a*, *b*, and γ in). Each unit cell is denoted by a number and a letter, where the number represents the number of Au atoms (solid cycles) in unit cell and the letter is used to distinguish different unit cells under the same number of Au atoms. Then, to consider the chain orientation effect for any given packing density of polymer brush, we further rotated 36 polymer chains from 0° to 360° by every 30° to describe different chain orientations. Thus, for a given polymer brush, a total of 348 packing structures were constructed and their packing energies were calculated and compared using MM.

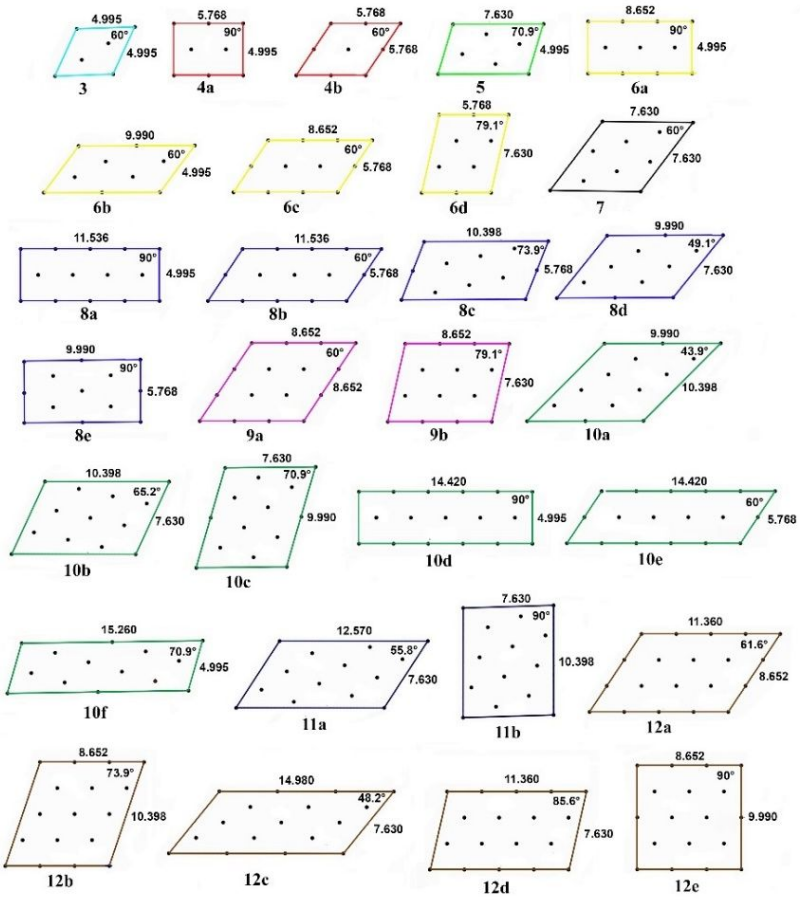

Figure 2. Schematic of twenty-nine unit cells used to accommodate a single chain and to present the packing density of polymer brushes. All of unit cells are defined by their lattice structural parameters (a, b, γ) and unit area as shown in this Figure and listed in **Table 1**. Each unit cell is denoted by an integer and a letter, where an integer represents the number of Au atoms (solid circles) per unit cell and a letter represent each distinct unit cell containing the same number of Au atoms.

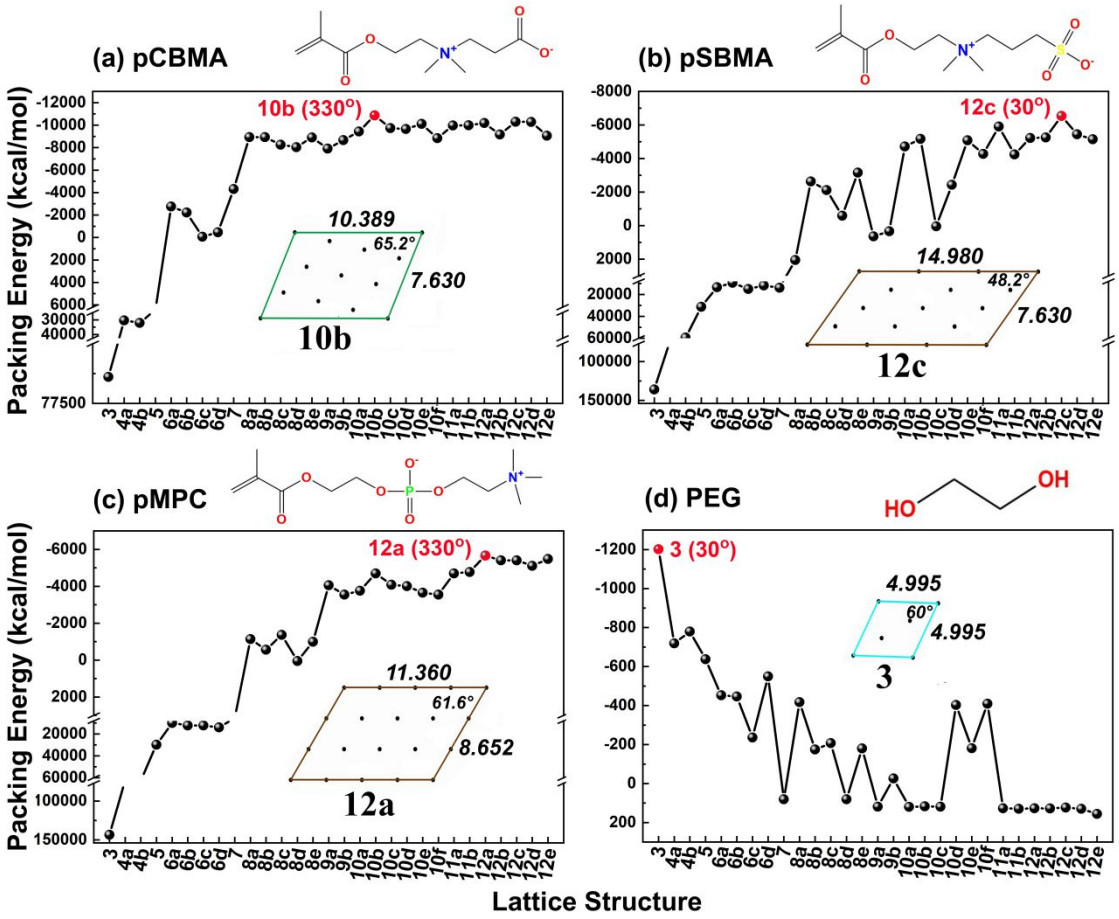

Figure 3. Searching for the optimal packing structures (red circles) of three zwitterionic and one PEG brushes. Packing energies of (a) pCBMA, (b) pSBMA, (c) pMPC, and (d) PEG brushes as a function of unit cells with already determined optimal chain orientation of polymer chains. For each unit cell, brush chain orientation is **considered by varying from 0° to 360° with an increase of 30°.**

Figure 3 shows the packing energies of three zwitterionic polymer (pCBMA, pSBMA, and pMPC) and one PEG brushes as a function of unit cells with the already determined optimal chain orientations from MM simulations. As shown in **Figure 3**, for all brush systems, there existed an optimal unit cell to better accommodate brush chains driven by the most energetically favorable chain-chain interactions. Generally, polymer brushes packed with too small unit cells (e.g. 3, 4a, 4b, and 5) led to unfavorable packing interactions due to the steric overpacking effect between large pendant groups, while the brushes with too large unit cells (e.g. 11a, 11b, 12a, 12b, 12c, 12d, and 12e) also lost some van der Waals (VDW) interactions due to the large separation distance between polymer chains. On the other hand, three zwitterionic polymer brushes (pCBMA, pSBMA, and pMPC) adopted distinct packing structure, showing a structure-dependent behavior. pCBMA containing two ethylene groups between zwitterionic groups reached the lowest packing energy at a unit cell of 10b with the optimal chain orientation of 330°, while pSBMA and pMPC with three ethylene groups between zwitterionic groups preferred to adopt the larger unit cells of 12c and 12d with the optimal chain orientations of 30° and

60°, respectively. Completely different from the three zwitterionic brushes, PEG brush with small ethylene glycol groups demonstrated energetical preference to adopt a typical $\sqrt{3}\times\sqrt{3}R30^{o}$ configuration with the chain orientation of 30°, consistent with several previous works[42, 46, 63]. As a result, the packing density was 72.0 $Å^2$ per pCBMA chain, 86.4 $Å^2$ per pSBMA chain, and 86.4 $Å^2$ per pMPC chain, all of which are 3-4 times larger than the packing density of PEG brushes (i.e., 21.6 $Å^2$ per PEG chain).

3.2. Interfacial water structures and dynamics on polymer brushes

On the basis of the "water barrier" hypothesis, it is generally accepted that the tightly bonded water layer near polymer brushes is critical for the antifouling performance, because structured and dynamic water at interfaces can greatly mediate protein adsorption[64]. Since it is not possible to use single or simple parameters derived from water behavior to well correlate the strength of bound water molecules to polymer chains with protein adsorption, the binding behavior of interfacial water molecules to polymer chains is characterized and measured by radial distribution function (RDF), coordinated number, orientation distribution, residence time, and self-diffusion coefficients of water molecules on polymer brushes.

Figure 4a shows radius distribution functions (RDFs) of interfacial water molecules on pCBMA, pSBMA, pMPC, and PEG brushes, where RDF presents the ratio of local water density to bulk water density as a function of the distance from the reference groups of polymer brushes. Oxygen atoms from PEG brush and zwitterionic groups (CO_2^-, SO_3^-, or PO_4^-) from the corresponding pCBMA, pSBMA, pMPC brushes were selected as reference points for RDFs. At the first glance, all pCBMA, pSBMA, pMPC, and PEG brushes exhibited two major peaks (i.e. first/second peaks) at the locations of 3.40/4.85 Å, 3.55/5.32 Å, 3.85/5.95 Å, and 2.85/4.75 Å, respectively, where the first hydration peak was much pronounced than the second one, indicating more water molecules in the first hydration layer than the second hydration layer. While pCBMA, pSBMA, and pMPC brushes had similar reference points for CO_2^-, SO_3^-, and PO_4^-, the two peak locations showed an increased order of pCBMA > pSBMA > pMPC. Packing density can also influence the distribution of water molecules at the surface. Along with a fact that pCBMA brush has the higher packing density than pSBMA and pMPC brushes, the shift of hydration peaks indicates that as compared to relatively loosely packed pSBMA and pMPC brushes, water molecules are still inclined to penetrate into the tightly packed pCBMA brush to form a more enriched hydration layer at the pCBMA surface. Next in **Figure 4b**, we quantified coordination number (N_w) of interfacial water molecules of pCBMA, pSBMA, pMPC, and PEG by integrating the first hydration shell of RDFs from **Figure 4a**. It can be seen in **Figure 4b** that N_w around pCBMA, pSBMA, and pMPC brushes were 5.54, 4.90, and 5.33, respectively, which were much higher than N_w=1.25 for PEG, confirming that zwitterionic moieties (e.g. -CB, -SB, and -PC) can induce the much stronger surface hydration than EG group. We attribute the structural differences in RDF shift and N_w between zwitterionic brushes and hydrophilic brushes to the different solvation mode, i.e., ionic solvation of zwitterionic polymer brushes induces the stronger hydration strength than hydrogen bonding solvation of hydrophilic polymer brushes.

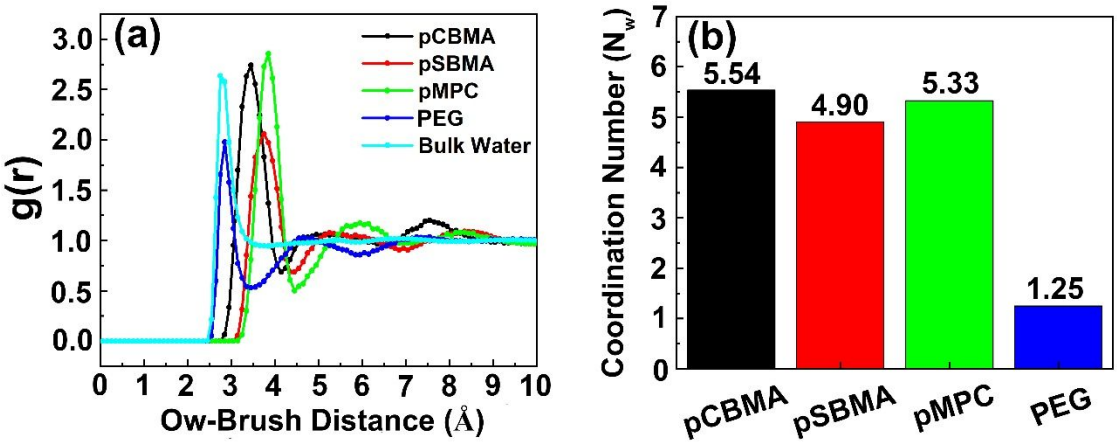

Figure 4. Interfacial water structures on the four polymer brushes. (a) RDFs and (b) coordination number (N_w) of interfacial water molecules on pCBMA, pSBMA, pMPC, and PEG brushes.

To characterize the orientation distribution of water molecules on the four different polymer brushes, we defined an angle θ between the dipole moment of water molecule and the brush normal, as illustrated in **Figure 5a**, where 0° (H-down) or 180° (H-up) indicates that a water molecule orients vertically relative to the surface with two hydrogens pointing towards or away from the surface, while 90° indicates a water molecule lie parallel to the surface. **Figure 5b** shows the orientation distribution of water molecules (θ) in the first hydration layer around the four different polymer brushes. As a control, θ obtained from bulk water had a broad and almost flat distribution, indicating a random orientation distribution of water molecules in bulk. Four θ profiles on polymer brushes displayed a single dominant peak, but with different maximal θ values, i.e., θ_{max}=100°, 100°, 130°, and 110° for pCBMA, pSBMA, pMPC, and PEG brushes, respectively. Since PEG brush tends to interact with water molecules via hydrogen bonds between oxygen atoms in EG groups and hydrogen atoms in water, interfacial water molecules had both H-up and H-down orientations on the surface. Differently, H-down oriented water molecules were preferentially located on pCMBA and pSBMA brushes, while H-up oriented water molecules tended to sit on the phosphate groups of pMPC brush (**Figure 5b**). Either case demonstrates a highly ordered behavior of water molecules occurring at the interface. Such difference in θ profiles is another indicator that interfacial water molecules adopt certain highly populated orientation to interact with polymer brushes relative to disordered bulk water.

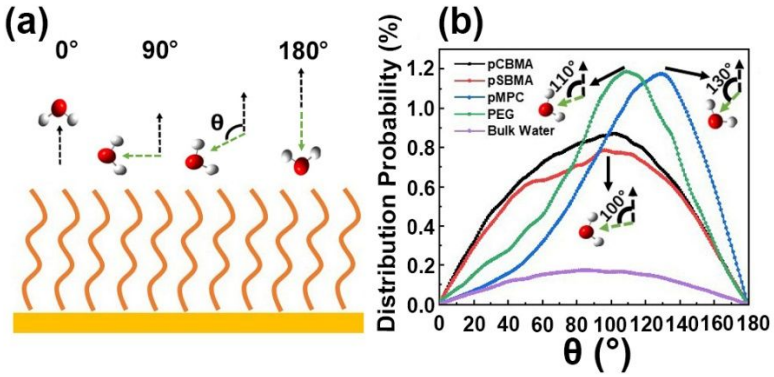

Figure 5. Water orientation distribution (θ) on pCBMA, pSBMA, pMPC, and PEG brushes. (a) Definition and (b) distribution probability of θ in the first hydration layer of the four polymer brushes.

Since the preferential water orientation is strongly depended on surface chemistry and structure of polymer brushes, we further quantified the structurally orientation of terminated zwitterionic groups of pCBMA (CO_2^- and NC_4^+), pSBMA (SO_3^- and NC_4^+), and pMPC (PO_4^- and NC_4^+) brushes. We defined an angle φ between the dipole moment of terminal zwitterionic moieties and the brush normal to quantify the averaged orientation of all zwitterionic moiety in brushes (**Figure 6a**). The dipole moment of terminal zwitterionic moieties was defined as positive groups (NC_4^+) orientating towards negative groups (CO_2^-, SO_3^-, and PO_4^-) of pCBMA, pSBMA, and pMPC.

The distribution probability profiles of φ in **Figure 6b** showed that the highly populated φ for pCBMA, pSBMA, and pMPC was peaked at 60°-90°, 90°, and 130° respectively. Despite difference in φ, further visual inspection of MD trajectories showed that all zwitterionic brushes formed a well-defined layer with relatively uniform thickness and top surface. It appeared that the zwitterionic groups dominated the chain orientation to retain the extended brush conformations. Meanwhile, to minimize the zwitterionic group-induced dipole on the brush surfaces, zwitterionic groups tended to adjust their orientations to have specific interactions with water molecules. pCBMA brush had up-tilted orientation of 60°-90° to facilitate negatively charged CO_2^- groups to interact with positively charged hydrogen atoms of water molecules. pSBMA brush adopted almost parallel orientation to the surface, which exposed more negatively charged sulfonate groups and hydrophobic CH_2 groups at the water–zwitterion interface while remaining the positively charged quaternary ammonium groups to stay largely in the inner region of the brush. Differently, pMPC (130°) had a completely opposite dipole from pCBMA (60°-90°) and pSBMA (90°), thus pMPC adopted down-titled orientation of 130° to better accommodation with water molecules to form a dense dipole network between positively charged NC_4^+ group of pMPC and negatively charged oxygen atoms of interfacial water molecules. Overall, comparison of the distribution probability of water orientation (θ) in **Figure 5b** with the dipole distribution of zwitterionic groups (φ) in **Figure 6b** confirms the formation of interfacial dipole network between zwitterionic groups and water molecules in the first hydration shell, which acts to minimize the surface dipoles and charges for enhancing surface hydration and possibly suppressing electrostatic/dipole-induced protein adsorption. A number of studies have showed that water molecules adopted both H-down and H-up

orientations at zwitterionic POPC/water interface[65-66]. Water strongly associated with the negatively charged PO_4^- with H-up orientation exhibited relatively stronger H-bond interaction with zwitterionic surface than that associated with positively charged NC_4^+ with H-down orientation, presumably due to the higher charge density of PO_4^- group (-1.2e) than NC_4^+ group (+0.78e). It was also reported that the positively charged surfaces are more favorable to interact with oxygen atoms of water molecules, while the negatively charged surfaces tend to interact with hydrogen atoms of water molecules[67-68], highlighting the importance of surface chemistry of the brushes in water orientation.

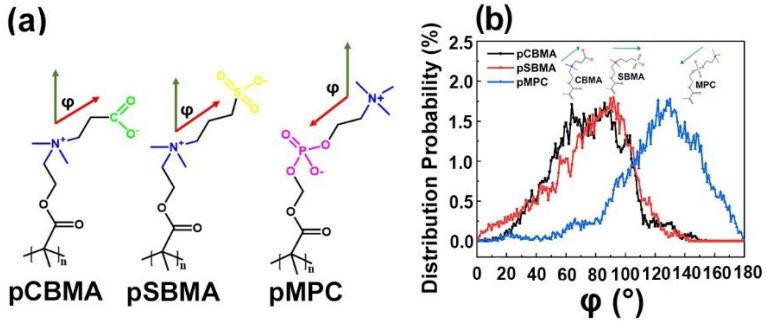

Figure 6. Dipole orientations of zwitterionic groups in pCBMA, pSBMA, and pMPC brushes. (a) Definition and (b) dipole distribution probability (%) of φ for pCBMA, pSMBA, and pMPC brushes. φ is an angle between a dipole of zwitterionic groups of pCBMA (60°-90°), pSBMA (90°), and pMPC (130°) and the brush normal.

From a dynamic viewpoint of a water hydration shell around different zwitterionic polymer brushes, we applied the mean residence time (MRT, **Figure 7a**) and self-diffusion coefficient (SDC, **Figure 7b**) to characterize the dynamics of interfacial water molecules in the first hydration layer of the four brushes. MRT (τ_s) is obtained by fitting an autocorrelation function of $C_R(t) = \frac{1}{N_w}\sum_{j=1}^{N_w} \frac{< P_{Rj}(0)P_{Rj}(t) >}{< P_{Rj}(0)^2 >}$ with $C_R(t) = Aexp(-\frac{t}{\tau_s})$, where P_{Rj} is a binary function and the value of 0 (1) presents that the *j*th water molecules stays (leaves) in a layer with a thickness of *R* at a time of *t*. A longer residence time (τ_s) indicates more stable water-polymer interactions, and vice versa. As shown in **Figure 7a**, the residence time of interfacial water molecules in the first hydration layer of pCBMA, pSBMA, pMPC, and PEG, as derived from a decay in a lifetime autocorrelation function, were 480 ps, 132 ps, 306 ps, and 63 ps, respectively, all of which were much longer than residence time of water molecules in bulk (40 ps), indicating the more stable association between polymers and water than water-water interactions. Water molecules bound to three zwitterionic brushes also exhibited 2-8 times longer τ_s than those bound to PEG brush, indicating that ionic solvation as induced by zwitterionic groups imposes the stronger interactions with water molecules than hydrogen bonds as induced by hydrophilic groups. The residence time is also strongly dependent on the electrostatic interactions between water molecules and the anionic groups, which rely on the charge densities of the anionic groups. Thus, we observed that τ_s for the three zwitterionic brushes exhibited a decreased order of pCBMA > pMPC > pSBMA, consistent with the coordination numbers of water molecules around zwitterionic brushes. In addition, carbon space length (CSL) may also affect the hydration structural and dynamic properties of these three zwitterionic groups.

pCBMA and pMPC with CSL=2 between zwitterionic groups had a longer τ_s of interfacial water molecules than pSBMA with CSL=3, probably because the smaller CSL=2 allows water molecules to form a bridge hydration layer between zwitterionic groups.

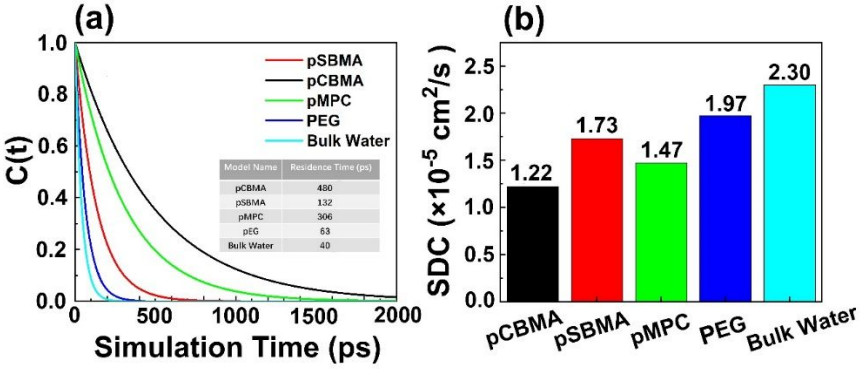

Figure 7. Interfacial water dynamics on polymer brushes. (a) Mean residence time (τ_s) and (b) self-diffusion coefficients (SDC) of interfacial water molecules in the first hydration shell of pCBMA, pSMBA, pMPC, and PEG brushes.

In parallel to τ_s, dynamically, surface-bound water molecules will be slowed by nearly any surface and the degree of slowing can be measured by water self-diffusion coefficients (SDC). Herein, we also examined the self-diffusion coefficient (SDC) of interfacial water molecules in the first hydration layer of pCBMA, pSBMA, pMPC, and PEG brushes by fitting a function of $\mathrm{SDC} = \lim_{t\to\infty} \frac{1}{6t} < [r_j(t) - r_j(0)]^2 >$, where $r_i(t)$ and $r_i(0)$ are the coordinates of the *j*th atom at time of *t* and *0,* respectively, and <⋯> indicates the ensemble average. As shown in **Figure 7b**, pCBMA, pSBMA, pMPC, and PEG exhibited the smaller SDC of 1.22×10^{-5}cm^2/s, 1.73×10^{-5}cm^2/s, 1.47×10^{-5} cm^2/s, and 1.97×10^{-5}cm^2/s than bulk water (2.30×10^{-5}cm^2/s), suggesting that all polymer brushes slow water diffusion considerably more than themselves. Among the four brushes, PEG-bound water molecules are more dynamics than zwitterionic-bound water molecules, as evidenced by the shorter τ_s and the larger SDC.

Obviously, the packing structure and surface chemistry of zwitterionic brushes (e.g. hydrophobicity/hydrophilicity ratio, charge distributions of cationic and anionic groups, and intra- or inter- interactions between zwitterionic groups) are greatly contributed to the structure and dynamics of water molecules, which are essential for understanding surface hydration and underlying polymer-water interactions. Collective simulation data from RDFs, coordination number, residence time, and self-diffusive coefficient showed consistent results on the structure and dynamics of interfacial water molecules. Zwitterionic brushes, particularly pCBMA, not only bind more water molecules, but also bind them the stronger and longer, than PEG brush, confirming that zwitterionic groups induce stronger surface hydration than hydrophilic groups. Among three zwitterionic brushes, different hydration properties are attributed to both zwitterionic groups and CSLs in zwitterionic polymer chains. Previous studies have shown that the hydration free energy and charge density of NC_4-CO_2 (-261±12 kJ/mol and -5.3 e/nm^3) were smaller than NC_4-SO_3 (-251±17 kJ/mol and -4.5 e/nm^3), indicating stronger surface free energy of -CB

moieties than -SB moieties[37, 69]. In addition, simulation results also showed the impact of CSL-induced surface hydration. pCBMA has a CSL of 2 between CO_2^- and NC_4^+ groups, while pSBMA and pMPC have a CSL of 3 between SO_3^- and NC_4^+ and between PO_4^- and NC_4^+. The increase of the number of CSL will increase a hydrophobicity/hydrophilicity ratio of zwitterionic chains and alter chain flexibility, both of which would lead to different water–polymer interactions to induce different surface hydration and antifouling behaviors for different polymer brushes. Also, CSL=2 in pCBMA has a separation distance of 3.8 Å, which allows water molecules to form bridging bonds between the two adjacent CO_2^- and NC_4^+ groups.

3.3. Protein adsorption/desorption on polymer brushes

Lysozyme is selected as a model foulant protein to quantify the degree of surface resistance of zwitterionic and PEG brushes. Protein adsorption process demands long timescale of seconds to hours in experiments, which is far beyond the timescale of 100 ns-μs of conventional molecular dynamics[70]. To overcome this timescale issue, we proposed two different computational strategies to study the lysozyme adsorption process on polymer brushes. The first strategy is to use a combination of Monte Carlo (MC) and MD simulations to study the lysozyme adsorption/desorption process on different polymer brushes, in which MC simulations were first performed to determine optimal orientation of a lysozyme on polymer brushes, followed all-atom, explicit-water MD simulations to determine the surface resistance to a lysozyme. **Figure 8** showed that after two-million steps of MC simulations, the optimal orientations of lysozyme on pCBMA, pSBMA, pMPC, and PEG brushes were determined at their lowest energy states.

Upon, at the lowest-, a lysozyme adopted a similar orientation with V-shape region of the lysozyme was oriented away from the three zwitterionic polymer brushes (**Figure 8**). However, we can also observe that lysozyme on PEG adopted a different orientation from the other three cases, with V-shape region of the lysozyme orientated towards the surface. Further, we characterized the residues of lysozyme orientating towards the brushes (**Table 2**). As shown in **Table 2**, some common residues of Arg_{125}, Gly_{126}, Cys_{127}, and Arg_{128} were found to face towards pCBMA and pSBMA brushes, which differed from the residue sequence of Thr_{118}-Asp_{119}-Gln_{121}-Ala_{122}-Trp_{123}-Ile_{124}-Arg_{125} orientating towards pMPC brush. All the above-mentioned residues adopted unstructured coil when facing to zwitterionic brushes. Differently, PEG brush induced the lysozyme to orient two regions of Thr_{118}-Asp_{119}-Gln_{121}-Ala_{122}-Trp_{123}-Ile_{124}-Arg_{125} (random coils) and Arg_{21}-Gly_{22}-Tyr_{23}-Ser_{24}-Leu_{25} (α-helical structure) towards the surface.

Table 2. Residues of lysozyme orientating towards pCBMA, pSBMA, pMPC, and PEG brushes from MC simulations.

	pCBMA	pSBMA	pMPC	PEG
Residues	Arg_{125} Gly_{126} Cys_{127} Arg_{128}	Arg_{125} Gly_{126} Cys_{127} Arg_{128}	Thr_{118} Asp_{119} Gln_{121} Ala_{122} Trp_{123} Ile_{124} Arg_{125}	Arg_{21} Gly_{22} Tyr_{23} Ser_{24} Leu_{25} Thr_{118} Asp_{119} Gln_{121} Ala_{122} Trp_{123} Ile_{124} Arg_{125}

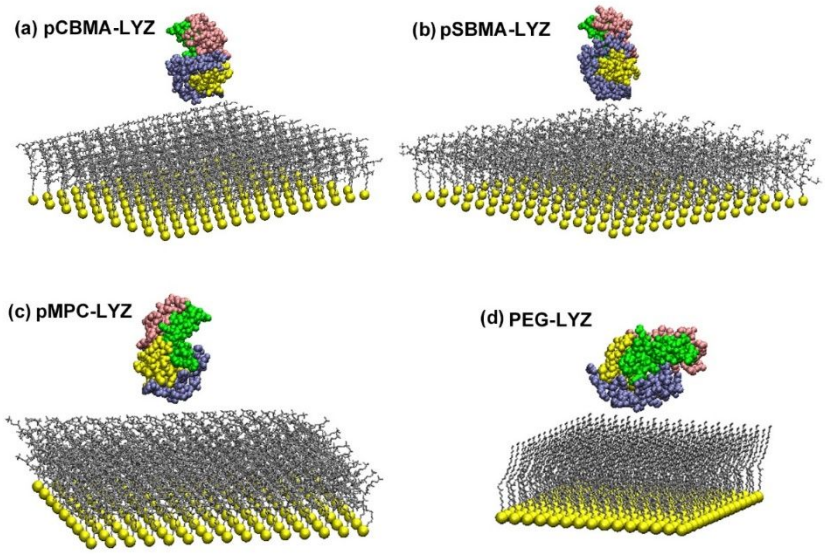

Figure 8. Optimal orientations of lysozyme on (a) pCBMA, (b) pSBMA, (c) pMPC, and (d) PEG brushes at the lowest energy state, as determined by MC simulations.

Upon obtaining the optimal orientations of a lysozyme on each polymer brush from MC simulations, we initiated the MD simulations by placing the lysozyme above the brush surface with a short separation distance of ~4 Å, which aims to mimic a pre-adsorption state. In this way, the less energy barrier is required for lysozyme to overcome in order to achieve its adsorption. If lysozyme is still rejected by polymer brushes, this further confirms the strong surface resistance property of a given polymer brush. **Figure 9** shows the relative positions of lysozyme relative to pCBMA, pSBMA, pMPC, and PEG surfaces as a function of simulation time, and final MD snapshots were also given to present the overall outcome of adsorption process. Visual inspection of 80-ns MD trajectories showed that as the simulation began, the lysozyme was quickly desorbed from the three zwitterionic brushes, as indicated by a large separation distance of 10-20 Å within 10 ns and final separation distance of 20-70 Å at 80 ns (**Figure 9a-c**), indicating the strong surface resistance of zwitterionic brushes to the lysozyme. In **Figure 9d**, different from zwitterionic brushes, lysozyme initially tended to weakly stay on the surface of PEG brush, as evidenced by a short separation distance of 0 to 5 Å within the first 45 ns. But after 45 ns, lysozyme gradually flied away from PEG brush. Furthermore, due to the desorption of lysozyme from the four polymer brushes, the secondary and tertiary structures of lysozyme were largely maintained.

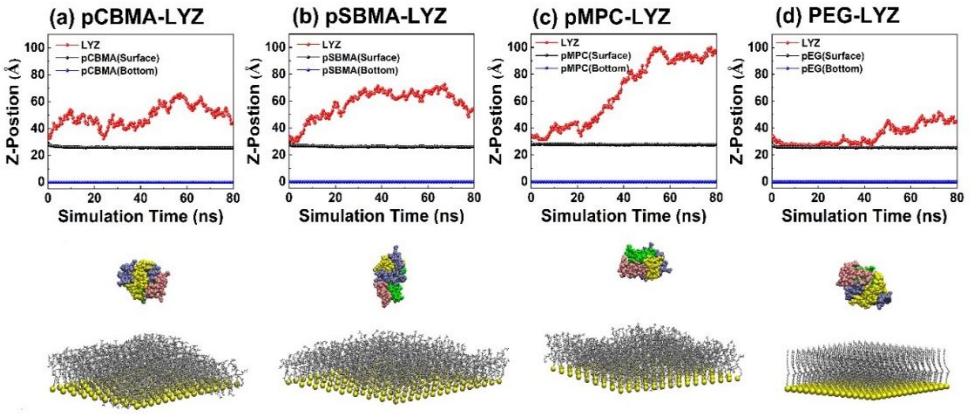

Figure 9. Time-dependent desorption process and final MD snapshots of lysozyme from (a) pCBMA, (b) pSBMA, (c) pMPC, and (d) PEG brushes.

We further proposed and implemented the second computational strategy to study the surface resistance ability to a lysozyme using steered molecular dynamic (SMD) simulations. **Figure 10a** illustrates the dynamical process of lysozyme approaching the polymer brushes from 14 Å to immediate contact of pCMBA, pSBMA, pMPC, and PEG brushes at a speed of 0.05 m/s by applying a harmonic force on the mass center of lysozyme. The driving speed of 0.05 m/s is slow enough to ensure an approximately quasistatic approach to the surface. During this process, the potential of mean force (PMF) can be obtained (**Figure 10b**) through the umbrella sampling method. As shown in **Figure 10b**, for all polymer brushes, there were no any repulsive force or attractive force acting on lysozyme when a separation distance between lysozyme and surface was larger than 9 Å. The nearly zero and flat force profiles also indicate that the lysozyme can readily approach any polymer brush without any anomalously high barriers. However, as lysozyme started to approach the brush surfaces from 14 Å to immediate contact of pCBMA and pMPC, pCBMA and pMPC brushes exhibited a significant increase of repulsive forces from 0 to -7000 pN and 0 to -5500 pN, respectively, indicating the strong surface resistance of both pCBMA and pMPC brushes to lysozyme adsorption. Differently, repulsive forces against lysozyme adsorption from pSBMA and PEG brushes were largely reduced to -2000 and -1000 pN, respectively, indicating that energy barriers for protein adsorption became much less pronounced.

To better understand the origin of repulsive forces from polymer brushes, we further analyzed repulsive force at the two special locations of hydration layers, at which the repulsive force begins to dramatically increase. As shown in **Figure 10c**, repulsive force on lysozyme at the first/second hydration layers was -2500/-700 pN for pCBMA, -500/-200 pN for pSBMA, -2500/-500 pN for pMPC, and -200/0 pN for PEG, respectively. This indicates that (1) repulsive force to break through the 2nd hydration layers by lysozyme was much smaller than that to break through the 1st hydration layers; (2) hydration layer indeed provides a physical and energetic barrier against protein adsorption; (3) repulsive forces from pCBMA and pMPC brushes were much higher than those from pSBMA and PEG brushes at both hydration layers. Particularly, repulsive force from pCBMA and pMPC brushes started to increase much earlier and steeper between two hydration layers, further

highlighting the stronger association of CO_2^- and PO_4^- groups with water molecules than SO_3^- and EG groups. A number of SPR results[71-72] have shown that the surfaces coated with pCBMA, pSBMA, and PEG brushes had protein adsorption from undiluted human blood serum/plasma of ~7.5/0.4 ng/cm^2, 45.1/9.1 ng/cm^2, and 87.5/>300.0 ng/cm^2, respectively, indicating pCBMA brush can achieve stronger antifouling ability to reject protein than pSBMA and PEG[71-74]. However, another quartz crystal microbalance (QCM) study has found that pCBMA, pSBMA, and pMPC brushes had protein adsorption of 79 ng/cm^2, 31 ng/cm^2, and 17 ng/cm^2 from undiluted fetal bovine serum, respectively[73], suggesting that pMPC outperformed the other two zwitterionic brushes in terms of antifouling capacity. Such controversial results for the same materials but from different labs could be resulted from different experimental conditions or measurable methods[73]. Moreover, it was reported that all of three pCBMA, pCBMA, and pMPC brushes can achieve very small water contact angle of <20°, with some minor differences between them (e.g. 13-15° for pCBMA brushes, 8-10° for pMPC brushes, and 19° for pSBMA brushes)[73]. Considering both simulation and experimental results together, zwitterionic brushes exhibit the stronger surface hydration and surface resistance to protein than PEG brush. Among three zwitterionic brushes, pCBMA and pMPC brushes outperform the other polymer brush to achieve the best surface hydration and protein resistance on the basis of an optimal combination of packing structures, zwitterionic groups, and CSLs.

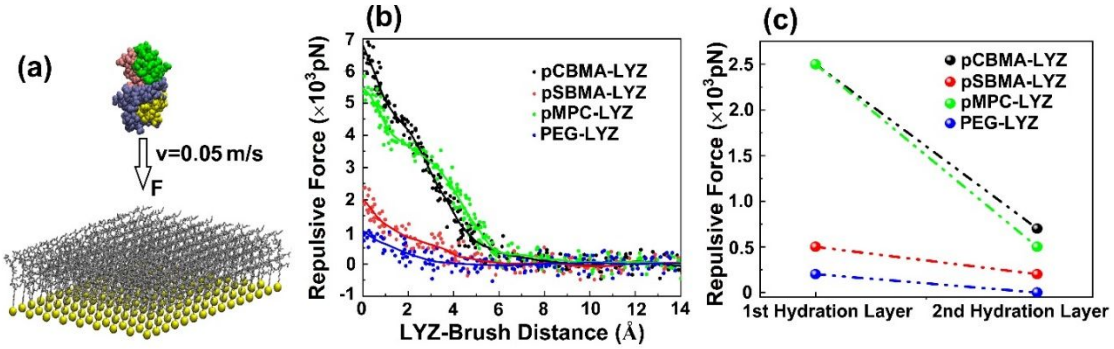

Figure 10. (a) Schematic of SMD simulations by pulling a lysozyme towards polymer brushes at a constant velocity of 0.05 m/s, (b) repulsive force-distance profiles between lysozyme and pCBMA, pSBMA, pMPC, and PEG brushes, and (c) repulsive force acting on lysozyme at the 1st and 2nd hydration layers of pCBMA, pSBMA, pMPC, and PEG brushes.

4. Conclusions

In this work, we computationally studied the packing structure, surface hydration, and surface resistance to protein of three zwitterionic polymer (pCBMA, pSBMA, and pMPC) brushes, as well as a PEG brush for a comparison using MM, MC, conventional MD, and SMD simulations, where MM was used to determine the optimal packing structures of the four polymer brushes, MC to predict optimal orientations of a lysozyme on the brushes, MD to examine the surface hydration and lysozyme adoption of the brushes, and SMD to quantify the repulsive force acting on a lysozyme from the brushes, respectively. Firstly, pCBMA, pSBMA, and pMPC brushes with the longer pendant sidechains energetically preferred to adopt much larger unit cells of 10b (a=10.395 Å, b=7.630 Å, γ=65.2°, Area=72.0 Å^2), 12c (a=14.980 Å, b=7.630 Å, γ=48.2°, Area=86.4

Å^2), 12a (a=11.360 Å, b=8.652 Å, γ=61.6°, Area=86.4 Å^2), respectively, in contrast to PEG brush with the smaller $\sqrt{3}\times\sqrt{3}R30°$ lattice structure. Upon obtaining optimal packing structures of polymer brushes, collective MD simulation data from RDFs, coordination number, dipole distribution, self-diffusion coefficient, and mean residence time of interfacial water molecules revealed the different binding strength and stability of interfacial waters to different brushes, as ranked by surface hydration in terms of pCBMA > pMPC > pSBMA > PEG. Finally, a combination of MD and SMD simulation studies further confirmed that while all brushes imposed strong surface resistance to lysozyme adsorption, repulsive forces acting on a lysozyme from the brushes was shown in a decreasing order of pCBMA > pMPC > pSBMA > PEG, consistent with the surface hydration order. Both orders reveal a positive relationship between surface hydration and antifouling properties of polymer brushes at atomic level. This computational work not only shows that subtle structural change in zwitterionic pendant groups but the same polymer backbone can greatly enhance antifouling performance, but also provide important structure-based design principles, in which combination of zwitterionic groups with optimal CSLs could serve as a promising structural motif for the design of new effective antifouling materials beyond traditional ethylene glycol-based antifouling materials

Acknowledgement. This work is supported by NSF grants (DMR-1806138 and CMMI-1825122). We also thank Aristo Liu (Copley High School) for his participation in this project.

Supporting Information. Force field parameters for pCBMA, pSBMA, and pMPC.

References

1. Jiang, S. Y.; Cao, Z. Q., Ultralow-Fouling, Functionalizable, and Hydrolyzable Zwitterionic Materials and Their Derivatives for Biological Applications. *Adv Mater* **2010,** *22* (9), 920-932.
2. Schlenoff, J. B., Zwitteration: Coating Surfaces with Zwitterionic Functionality to Reduce Nonspecific Adsorption. *Langmuir* **2014,** *30* (32), 9625-9636.
3. Georgiev, G. S.; Kamenska, E. B.; Vassileva, E. D.; Kamenova, I. P.; Georgieva, V. T.; Iliev, S. B.; Ivanov, I. A., Self-assembly, antipolyelectrolyte effect, and nonbiofouling properties of polyzwitterions. *Biomacromolecules* **2006,** *7* (4), 1329-1334.
4. Xiao, S. W.; Ren, B. P.; Huang, L.; Shen, M. X.; Zhang, Y. X.; Zhong, M. Q.; Yang, J. T.; Zheng, J., Salt-responsive zwitterionic polymer brushes with anti-polyelectrolyte property. *Curr Opin Chem Eng* **2018,** *19*, 86-93.
5. Xiao, S. W.; Zhang, Y. X.; Shen, M. X.; Chen, F.; Fan, P.; Zhong, M. Q.; Ren, B. P.; Yang, J. T.; Zheng, J., Structural Dependence of Salt-Responsive Polyzwitterionic Brushes with an Anti-Polyelectrolyte Effect. *Langmuir* **2018,** *34* (1), 97-105.
6. Wei, R.; Song, W. Y.; Yang, F.; Zhou, J. K.; Zhang, M.; Zhang, X.; Zhao, W. F.; Zhao, C. S., Bidirectionally pH-Responsive Zwitterionic Polymer Hydrogels with Switchable Selective Adsorption Capacities for Anionic and Cationic Dyes. *Ind Eng Chem Res* **2018,** *57* (24), 8209-8219.
7. Wu, J.; He, C. C.; He, H. C.; Cheng, C. Q.; Zhu, J. Y.; Xiao, Z. C.; Zhang, H. Y.; Li, X. K.; Zheng, J.; Xiao, J., Importance of zwitterionic incorporation into polymethacrylate-based hydrogels for simultaneously improving optical transparency, oxygen permeability, and antifouling properties. *J Mater Chem B* **2017,** *5* (24), 4595-4606.
8. Cao, B.; Tang, Q.; Li, L. L.; Humble, J.; Wu, H. Y.; Liu, L. Y.; Cheng, G., Switchable Antimicrobial and Antifouling Hydrogels with Enhanced Mechanical Properties. *Adv Healthc Mater* **2013,** *2* (8), 1096-1102.
9. Durrani, A. A.; Hayward, J. A.; Chapman, D., Biomembranes as Models for Polymer Surfaces .2. The Syntheses of Reactive Species for Covalent Coupling of Phosphorylcholine to Polymer Surfaces. *Biomaterials* **1986,** *7* (2), 121-125.
10. Tang, Y.; Lu, J. R.; Lewis, A. L.; Vick, T. A.; Stratford, P. W., Swelling of zwitterionic polymer films characterized by spectroscopic ellipsometry. *Macromolecules* **2001,** *34* (25), 8768-8776.
11. Liu, J. X.; Yang, K. G.; Shao, W. Y.; Li, S. W.; Wu, Q.; Zhang, S.; Qu, Y. Y.; Zhang, L. H.; Zhang, Y. K., Synthesis of Zwitterionic Polymer Particles via Combined Distillation Precipitation Polymerization and Click Chemistry for Highly Efficient Enrichment of Glycopeptide. *Acs Appl Mater Inter* **2016,** *8* (34), 22018-22024.
12. Ventura, C.; Guerin, A. J.; El-Zubir, O.; Ruiz-Sanchez, A. J.; Dixon, L. I.; Reynolds, K. J.; Dale, M. L.; Ferguson, J.; Houlton, A.; Horrocks, B. R.; Clare, A. S.; Fulton, D. A., Marine antifouling performance of polymer coatings incorporating zwitterions. *Biofouling* **2017,** *33* (10), 892-903.
13. Xiao, S. W.; Yang, Y.; Zhong, M. Q.; Chen, H.; Zhang, Y. X.; Yang, J. T.; Zheneg, J., Salt-Responsive Bilayer Hydrogels with Pseudo-Double-Network Structure Actuated by Polyelectrolyte and Antipolyelectrolyte Effects. *Acs Appl Mater Inter* **2017,** *9* (24), 20843-20851.
14. Xiao, S. W.; Zhang, M. Z.; He, X. M.; Huang, L.; Zhang, Y. X.; Ren, B. P.; Zhong, M. Q.; Chang, Y.; Yang, J. T.; Zheng, J., Dual Salt- and Thermoresponsive Programmable Bilayer Hydrogel Actuators with Pseudo-Interpenetrating Double-Network Structures. *Acs Appl Mater Inter* **2018,** *10* (25), 21642-21653.
15. Maji, T.; Banerjee, S.; Biswas, Y.; Mandal, T. K., Dual-Stimuli-Responsive L-Serine-Based Zwitterionic UCST-Type Polymer with Tunable Thermosensitivity. *Macromolecules* **2015,** *48* (14), 4957-4966.

16. Hisamatsu, Y.; Banerjee, S.; Avinash, M. B.; Govindaraju, T.; Schmuck, C., A Supramolecular Gel from a Quadruple Zwitterion that Responds to Both Acid and Base. *Angew Chem Int Edit* **2013,** *52* (48), 12550-12554.
17. Bai, T.; Liu, S. J.; Sun, F.; Sinclair, A.; Zhang, L.; Shao, Q.; Jiang, S. Y., Zwitterionic fusion in hydrogels and spontaneous and time-independent self-healing under physiological conditions. *Biomaterials* **2014,** *35* (13), 3926-3933.
18. Chen, M.; Briscoe, W. H.; Armes, S. P.; Cohen, H.; Klein, J., Polyzwitterionic brushes: Extreme lubrication by design. *Eur Polym J* **2011,** *47* (4), 511-523.
19. Kobayashi, M.; Terayama, Y.; Hosaka, N.; Kaido, M.; Suzuki, A.; Yamada, N.; Torikai, N.; Ishihara, K.; Takahara, A., Friction behavior of high-density poly(2-methacryloyloxyethyl phosphorylcholine) brush in aqueous media. *Soft Matter* **2007,** *3* (6), 740-746.
20. Jorgensen, W. L.; Chandrasekhar, J.; Madura, J. D.; Impey, R. W.; Klein, M. L., Comparison of Simple Potential Functions for Simulating Liquid Water. *J Chem Phys* **1983,** *79* (2), 926-935.
21. Li, B. W.; Yuan, Z. F.; Zhang, P.; Sinclair, A.; Jain, P.; Wu, K.; Tsao, C.; Xie, J. Y.; Hung, H. C.; Lin, X. J.; Bai, T.; Jiang, S. Y., Zwitterionic Nanocages Overcome the Efficacy Loss of Biologic Drugs. *Adv Mater* **2018,** *30* (14), 1705728.
22. Blackman, L. D.; Gunatillake, P. A.; Cass, P.; Locock, K. E. S., An introduction to zwitterionic polymer behavior and applications in solution and at surfaces. *Chem Soc Rev* **2019,** *48* (3), 757-770.
23. Chou, Y. N.; Sun, F.; Hung, H. C.; Jain, P.; Sinclair, A.; Zhang, P.; Bai, T.; Chang, Y.; Wen, T. C.; Yu, Q. M.; Jiang, S. Y., Ultra-low fouling and high antibody loading zwitterionic hydrogel coatings for sensing and detection in complex media. *Acta Biomater* **2016,** *40*, 31-37.
24. Yang, W.; Bai, T.; Carr, L. R.; Keefe, A. J.; Xu, J. J.; Xue, H.; Irvin, C. A.; Chen, S. F.; Wang, J.; Jiang, S. Y., The effect of lightly crosslinked poly(carboxybetaine) hydrogel coating on the performance of sensors in whole blood. *Biomaterials* **2012,** *33* (32), 7945-7951.
25. Liu, J.; Zhou, J., Hydrolysis-controlled protein adsorption and antifouling behaviors of mixed charged self-assembled monolayer: A molecular simulation study. *Acta Biomater* **2016,** *40*, 23-30.
26. Chang, Y.; Shu, S. H.; Shih, Y. J.; Chu, C. W.; Ruaan, R. C.; Chen, W. Y., Hemocompatible Mixed-Charge Copolymer Brushes of Pseudozwitterionic Surfaces Resistant to Nonspecific Plasma Protein Fouling. *Langmuir* **2010,** *26* (5), 3522-3530.
27. Liu, X. S.; Huang, H. Y.; Jin, Q.; Ji, J., Mixed Charged Zwitterionic Self-Assembled Monolayers as a Facile Way to Stabilize Large Gold Nanoparticles. *Langmuir* **2011,** *27* (9), 5242-5251.
28. Chen, S.; Zheng, J.; Li, L.; Jiang, S., Strong resistance of phosphorylcholine self-assembled monolayers to protein adsorption: insights into nonfouling properties of zwitterionic materials. *Journal of the American Chemical Society* **2005,** *127* (41), 14473-14478.
29. Chang, Y.; Liao, S. C.; Higuchi, A.; Ruaan, R. C.; Chu, C. W.; Chen, W. Y., A Highly stable nonbiofouling surface with well-packed grafted zwitterionic polysulfobetaine for plasma protein repulsion. *Langmuir* **2008,** *24* (10), 5453-5458.
30. Vaisocherova, H.; Zhang, Z.; Yang, W.; Cao, Z. Q.; Cheng, G.; Taylor, A. D.; Piliarik, M.; Homola, J.; Jiang, S. Y., Functionalizable surface platform with reduced nonspecific protein adsorption from full blood plasma-Material selection and protein immobilization optimization. *Biosens Bioelectron* **2009,** *24* (7), 1924-1930.
31. Ilcikova, M.; Tkac, J.; Kasak, P., Switchable Materials Containing Polyzwitterion Moieties. *Polymers-Basel* **2015,** *7* (11), 2344-2370.
32. Chen, S. F.; Li, L. Y.; Zhao, C.; Zheng, J., Surface hydration: Principles and applications toward low-fouling/nonfouling biomaterials. *Polymer* **2010,** *51* (23), 5283-5293.

33. Higaki, Y.; Nishida, J.; Takenaka, A.; Yoshimatsu, R.; Kobayashi, M.; Takahara, A., Versatile inhibition of marine organism settlement by zwitterionic polymer brushes. *Polym J* **2015,** *47* (12), 811-818.
34. Zhao, W. W.; Ye, Q.; Hu, H. Y.; Wang, X. L.; Zhou, F., Grafting zwitterionic polymer brushes via electrochemical surface-initiated atomic-transfer radical polymerization for anti-fouling applications. *J Mater Chem B* **2014,** *2* (33), 5352-5357.
35. Chen, H.; Yang, J. T.; Xiao, S. W.; Hu, R. D.; Bhaway, S. M.; Vogt, B. D.; Zhang, M. Z.; Chen, Q.; Ma, J.; Chang, Y.; Li, L. Y.; Zheng, J., Salt-responsive polyzwitterionic materials for surface regeneration between switchable fouling and antifouling properties. *Acta Biomater* **2016,** *40*, 62-69.
36. Yang, J. T.; Chen, H.; Xiao, S. W.; Shen, M. X.; Chen, F.; Fan, P.; Zhong, M. Q.; Zheng, J., Salt-Responsive Zwitterionic Polymer Brushes with Tunable Friction and Antifouling Properties. *Langmuir* **2015,** *31* (33), 9125-9133.
37. Shao, Q.; Jiang, S., Influence of Charged Groups on the Properties of Zwitterionic Moieties: A Molecular Simulation Study. *The Journal of Physical Chemistry B* **2014,** *118* (27), 7630-7637.
38. Shao, Q.; He, Y.; White, A. D.; Jiang, S. Y., Difference in Hydration between Carboxybetaine and Sulfobetaine. *J Phys Chem B* **2010,** *114* (49), 16625-16631.
39. Liu, Z. Y.; Jiang, Q.; Jin, Z. Q.; Sun, Z. Y.; Ma, W. J.; Wang, Y. L., Understanding the Antifouling Mechanism of Zwitterionic Monomer-Grafted Polyvinylidene Difluoride Membranes: A Comparative Experimental and Molecular Dynamics Simulation Study. *Acs Applied Materials & Interfaces* **2019,** *11* (15), 14408-14417.
40. He, Y.; Shao, Q.; Tsao, H.-K.; Chen, S.; Goddard, W. A.; Jiang, S., Understanding Three Hydration-Dependent Transitions of Zwitterionic Carboxybetaine Hydrogel by Molecular Dynamics Simulations. *The Journal of Physical Chemistry B* **2011,** *115* (40), 11575-11580.
41. He, Y.; Tsao, H. K.; Jiang, S. Y., Improved Mechanical Properties of Zwitterionic Hydrogels with Hydroxyl Groups. *J Phys Chem B* **2012,** *116* (19), 5766-5770.
42. Zheng, J.; Li, L.; Chen, S.; Jiang, S., Molecular simulation study of water interactions with oligo (ethylene glycol)-terminated alkanethiol self-assembled monolayers. *Langmuir* **2004,** *20* (20), 8931-8938.
43. Zheng, J.; Li, L.; Tsao, H.-K.; Sheng, Y.-J.; Chen, S.; Jiang, S., Strong Repulsive Forces between Protein and Oligo (Ethylene Glycol) Self-Assembled Monolayers: A Molecular Simulation Study. *Biophysical Journal* **2005,** *89* (1), 158-166.
44. Zheng, J.; He, Y.; Chen, S.; Li, L.; Bernards, M. T.; Jiang, S., Molecular simulation studies of the structure of phosphorylcholine self-assembled monolayers. *J Chem Phys* **2006,** *125* (17), 174714.
45. Zhang, Z.; Vaisocherova, H.; Cheng, G.; Yang, W.; Xue, H.; Jiang, S. Y., Nonfouling Behavior of Polycarboxybetaine-Grafted Surfaces: Structural and Environmental Effects. *Biomacromolecules* **2008,** *9* (10), 2686-2692.
46. Zhou, J.; Zheng, J.; Jiang, S. Y., Molecular simulation studies of the orientation and conformation of cytochrome c adsorbed on self-assembled monolayers. *J Phys Chem B* **2004,** *108* (45), 17418-17424.
47. He, Y.; Hower, J.; Chen, S. F.; Bernards, M. T.; Chang, Y.; Jiang, S. Y., Molecular simulation studies of protein interactions with zwitterionic phosphorylcholine self-assembled monolayers in the presence of water. *Langmuir* **2008,** *24* (18), 10358-10364.
48. Cheung, D. L.; Lau, K. H. A., Atomistic Study of Zwitterionic Peptoid Antifouling Brushes. *Langmuir* **2019,** *35* (5), 1483-1494.

49. Xiang, Y.; Xu, R. G.; Leng, Y. S., Molecular Simulations of the Hydration Behavior of a Zwitterion Brush Array and Its Antifouling Property in an Aqueous Environment. *Langmuir* **2018,** *34* (6), 2245-2257.
50. Vanommeslaeghe, K.; Hatcher, E.; Acharya, C.; Kundu, S.; Zhong, S.; Shim, J.; Darian, E.; Guvench, O.; Lopes, P.; Vorobyov, I.; Mackerell, A. D., Jr., CHARMM general force field: A force field for drug-like molecules compatible with the CHARMM all-atom additive biological force fields. *J. Comput. Chem.* **2010,** *31* (4), 671-690.
51. Klauda, J. B.; Venable, R. M.; Freites, J. A.; O'Connor, J. W.; Tobias, D. J.; Mondragon-Ramirez, C.; Vorobyov, I.; MacKerell, A. D.; Pastor, R. W., Update of the CHARMM All-Atom Additive Force Field for Lipids: Validation on Six Lipid Types. *The Journal of Physical Chemistry B* **2010,** *114* (23), 7830-7843.
52. Vorobyov, I.; Anisimov, V. M.; Greene, S.; Venable, R. M.; Moser, A.; Pastor, R. W.; MacKerell, A. D., Additive and Classical Drude Polarizable Force Fields for Linear and Cyclic Ethers. *Journal of Chemical Theory and Computation* **2007,** *3* (3), 1120-1133.
53. Herzberg, O.; Sussman, J. L., Protein Model-Building by the Use of a Constrained-Restrained Least-Squares Procedure. *J Appl Crystallogr* **1983,** *16* (Feb), 144-150.
54. Phillips, J. C.; Braun, R.; Wang, W.; Gumbart, J.; Tajkhorshid, E.; Villa, E.; Chipot, C.; Skeel, R. D.; Kale, L.; Schulten, K., Scalable molecular dynamics with NAMD. *J Comput Chem* **2005,** *26* (16), 1781-1802.
55. Werber, J. R.; Osuji, C. O.; Elimelech, M., Materials for next-generation desalination and water purification membranes. *Nature Reviews Materials* **2016,** *1* (5), 1-15.
56. Liu, C. H.; Lee, J.; Small, C.; Ma, J.; Elimelech, M., Comparison of organic fouling resistance of thin-film composite membranes modified by hydrophilic silica nanoparticles and zwitterionic polymer brushes. *J Membrane Sci* **2017,** *544*, 135-142.
57. Graham, M. V.; Mosier, A. P.; Kiehl, T. R.; Kaloyeros, A. E.; Cady, N. C., Development of antifouling surfaces to reduce bacterial attachment. *Soft Matter* **2013,** *9* (27), 6235-6244.
58. Schumacher, J. F.; Carman, M. L.; Estes, T. G.; Feinberg, A. W.; Wilson, L. H.; Callow, M. E.; Callow, J. A.; Finlay, J. A.; Brennan, A. B., Engineered antifouling microtopographies–effect of feature size, geometry, and roughness on settlement of zoospores of the green alga Ulva. *Biofouling* **2007,** *23* (1), 55-62.
59. Xiao, S.; Ren, B.; Huang, L.; Shen, M.; Zhang, Y.; Zhong, M.; Yang, J.; Zheng, J., Salt-responsive zwitterionic polymer brushes with anti-polyelectrolyte property. *Current Opinion in Chemical Engineering* **2018,** *19*, 86-93.
60. Xiao, S.; Zhang, Y.; Shen, M.; Chen, F.; Fan, P.; Zhong, M.; Ren, B.; Yang, J.; Zheng, J., Structural dependence of salt-responsive polyzwitterionic brushes with an anti-polyelectrolyte effect. *Langmuir* **2018,** *34* (1), 97-105.
61. Yang, F. Y.; Liu, Y. L.; Zhang, Y. X.; Ren, B. P.; Xu, J. X.; Zheng, J., Synthesis and Characterization of Ultralow Fouling Poly(N-acryloyl-glycinamide) Brushes. *Langmuir* **2017,** *33* (49), 13964-13972.
62. Herrwerth, S.; Eck, W.; Reinhardt, S.; Grunze, M., Factors that Determine the Protein Resistance of Oligoether Self-Assembled Monolayers − Internal Hydrophilicity, Terminal Hydrophilicity, and Lateral Packing Density. *J Am Chem Soc* **2003,** *125* (31), 9359-9366.
63. Li, L.; Chen, S.; Zheng, J.; Ratner, B. D.; Jiang, S., Protein adsorption on oligo(ethylene glycol)-terminated alkanethiolate self-assembled monolayers: the molecular basis for nonfouling behavior. *J. Phys. Chem. B* **2005,** *109* (7), 2934-2941.
64. Zhang, Y.; Liu, Y.; Ren, B.; Zhang, D.; Xie, S.; Chang, Y.; Yang, J.; Wu, J.; Xu, L.; Zheng, J., Fundamentals and applications of zwitterionic antifouling polymers. *Journal of Physics D: Applied Physics* **2019,** *52* (40), 403001.

65. Mondal, J. A.; Nihonyanagi, S.; Yamaguchi, S.; Tahara, T., Three Distinct Water Structures at a Zwitterionic Lipid/Water Interface Revealed by Heterodyne-Detected Vibrational Sum Frequency Generation. *J Am Chem Soc* **2012,** *134* (18), 7842-7850.
66. Re, S. Y.; Nishima, W.; Tahara, T.; Sugita, Y., Mosaic of Water Orientation Structures at a Neutral Zwitterionic Lipid/Water Interface Revealed by Molecular Dynamics Simulations (vol 5, pg 4343, 2014). *J Phys Chem Lett* **2015,** *6* (1), 195-195.
67. Lis, D.; Backus, E. H. G.; Hunger, J.; Parekh, S. H.; Bonn, M., Liquid flow along a solid surface reversibly alters interfacial chemistry. *Science* **2014,** *344* (6188), 1138-1142.
68. Mondal, J. A.; Nihonyanagi, S.; Yamaguchi, S.; Tahara, T., Structure and Orientation of Water at Charged Lipid Monolayer/Water Interfaces Probed by Heterodyne-Detected Vibrational Sum Frequency Generation Spectroscopy. *J Am Chem Soc* **2010,** *132* (31), 10656-10657.
69. Shao, Q.; Mi, L.; Han, X.; Bai, T.; Liu, S. J.; Li, Y. T.; Jiang, S. Y., Differences in Cationic and Anionic Charge Densities Dictate Zwitterionic Associations and Stimuli Responses. *J Phys Chem B* **2014,** *118* (24), 6956-6962.
70. Quan, X. B.; Liu, J.; Zhou, J., Multiscale modeling and simulations of protein adsorption: progresses and perspectives. *Curr Opin Colloid In* **2019,** *41*, 74-85.
71. Zhang, Z.; Zhang, M.; Chen, S. F.; Horbetta, T. A.; Ratner, B. D.; Jiang, S. Y., Blood compatibility of surfaces with superlow protein adsorption. *Biomaterials* **2008,** *29* (32), 4285-4291.
72. Ladd, J.; Zhang, Z.; Chen, S.; Hower, J. C.; Jiang, S., Zwitterionic polymers exhibiting high resistance to nonspecific protein adsorption from human serum and plasma. *Biomacromolecules* **2008,** *9* (5), 1357-1361.
73. Inoue, Y.; Ishihara, K., Reduction of protein adsorption on well-characterized polymer brush layers with varying chemical structures. *Colloids and Surfaces B: Biointerfaces* **2010,** *81* (1), 350-357.
74. Emmenegger, C. R.; Brynda, E.; Riedel, T.; Sedlakova, Z.; Houska, M.; Alles, A. B., Interaction of Blood Plasma with Antifouling Surfaces. *Langmuir* **2009,** *25* (11), 6328-6333.

Figure of Content